THE JOURNAL OF PHYSICAL CHEMISTRY LETTERS
A JOURNAL OF THE AMERICAN CHEMICAL SOCIETY

pubs.acs.org/JPCL Letter

First-Principles Calculation of the Temperature-Dependent Transition Energies in Spin Defects

Hao Tang, Ariel Rebekah Barr, Guoqing Wang, Paola Cappellaro,* and Ju Li*

Cite This: J. Phys. Chem. Lett. 2023, 14, 3266−3273 Read Online

ACCESS | Metrics & More | Article Recommendations | Supporting Information

ABSTRACT: Spin qubits associated with color centers are promising platforms for various quantum technologies. However, to be deployed in robust quantum devices, the variations of their intrinsic properties with the external conditions, in particular temperature and strain, should be known with high precision. Unfortunately, a predictive theory on the temperature dependence of the resonance frequency of electron and nuclear spin defects in solids remains lacking. In this work, we develop a first-principles method for the temperature dependence of the zero-field splitting, hyperfine interaction, and nuclear quadrupole interaction of color centers. As a testbed, we compare our ab initio calculations with experiments for the nitrogen-vacancy (NV^-) center in diamond, finding good agreements. We identify the major origin of the temperature dependence as a second-order effect of dynamic phonon vibrations, instead of the thermal-expansion strain. The method can be applied to different color centers and provides a theoretical tool for designing high-precision quantum sensors.

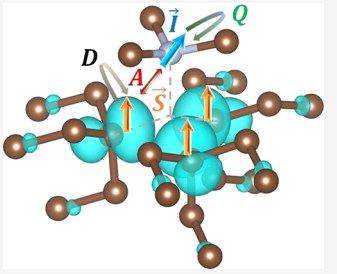

Color centers, the fluorescent lattice defects in insulators, have been intensively studied as solid-state qubits for quantum computing,[1,2] quantum communication,[3,4] and quantum sensing.[5,6] The temperature (and strain) dependence of the spin defect properties is a critical factor in their performance: their spatiotemporal fluctuations in the crystal host would result in degraded coherence times, while the sensitivity of the defects to their small variations can be exploited in quantum sensing.[5] A predictive theoretical model accompanied by a robust computational protocol would be invaluable in both mitigating deleterious effects and selecting the best host/defect combinations for quantum sensing. Here, we developed a first-principles method for predicting the temperature dependence of optical, electronic, and nuclear spin-transition frequencies. We benchmark our calculations using the properties of the nitrogen-vacancy (NV^-) center in diamond. Our first-principles calculations achieve excellent agreement with the temperature dependence of the NV^- zero phonon line (ZPL), zero-field splitting (ZFS), hyperfine interaction, and nuclear quadrupole interaction. Crucially, we find that the dominant part of the temperature dependence is from a second-order dynamical phonon effect. Our method paves the way for computation-assisted design of novel quantum sensors using color centers in solids.

We select the NV^- center as our testbed, since it has been accurately characterized in experiments for its applications to quantum sensing of magnetic fields,[7−9] electric fields,[10] temperature,[11,12] pressure,[13,14] and rotation.[15,16] While the temperature dependence of the NV^- electronic spin resonance frequency[17] has been exploited to probe the local temperature with ultrahigh spatial resolution in nanothermometry devices,[18−25] it is also detrimental to some quantum devices, since its fluctuations can lead to decoherence.[26]

Despite extensive experimental study on the temperature dependence of both electronic and nuclear spin frequencies,[27−32] a predictive theoretical method is still lacking. The temperature dependence has been previously attributed to the thermal-expansion strain, but the calculated temperature shifts are far smaller in absolute magnitude than the experimental values[27,31−33] (approximately by an order of magnitude). This discrepancy indicates that other effects dominate the temperature dependence. Various explanations have being proposed for such a discrepancy. Doherty et al. proposed that the dynamical phonon effect might play an important role in the temperature dependence of the ZFS.[17] However, in the absence of a method to evaluate the dynamical phonon effect from first-principles, its contribution to the temperature dependence could not be unambiguously determined. To overcome these challenges, here we develop a theoretical model of the defect transition energy ν dependence on the temperature-induced atomic displacement up to the second order. We combine a full calculation of the phonon spectrum including density functional perturbation theory (DFPT)[34] with density functional theory (DFT) calculation of the spin-transition energies with the supercell method.[35]

Given an electron−nuclear spin system, such as the NV^- center, we aim at calculating the temperature-induced shift of a transition frequency ν between any two levels that can be

Received: February 2, 2023
Accepted: March 22, 2023
Published: March 28, 2023

https://doi.org/10.1021/acs.jpclett.3c00314
J. Phys. Chem. Lett. 2023, 14, 3266−3273

probed experimentally (e.g., by Rabi experiments.) The shift in ν arises from the temperature-induced atomic displacement, as the thermal excitation of electrons is negligible due to the large energy gap in a broad temperature range. For a general transition, the atomic displacement effect is described by the energy surfaces of the two levels as a function of atomic coordinates, as shown in Figure 1(a). Expressing the atomic

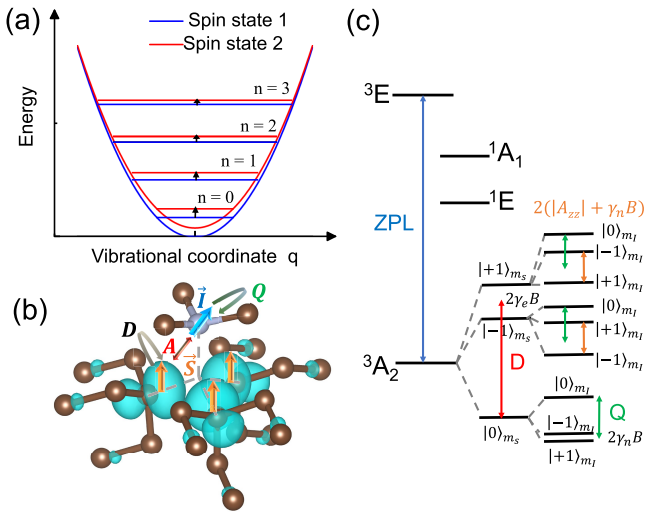

Figure 1. (a) Illustration of the second-order phonon effect to spin resonance. (b) Electron and nuclear spin interaction in an NV^- center. The blue isosurface of electron spin density is from the DFT, and the brown and silver spheres represent carbon and nitrogen atoms, respectively. (c) The energy levels of NV^- centers.

configuration by the normal coordinates of phonon modes $\{q_i\}$, the transition frequency is then a function of $(\{q_i\})$: $\nu(\{q_i\}) \equiv [E_2(\{q_i\}) - E_1(\{q_i\})]/h$ (E_1 and E_2 are the energy level 1 and energy level 2, respectively). At finite temperature, $\{q_i\}$ has both thermal and quantum fluctuations. As all electron and nuclear spin-transition frequencies (zero-field splitting D, hyperfine interaction A, and nuclear quadrupole interaction Q) are at least 3 orders of magnitude smaller than the typical phonon frequency,[36] the measured ν is a statistical average over the phonon mode distribution:

$$\langle \nu \rangle = \nu_0 + \sum_i \left[\left. \frac{\partial \nu}{\partial q_i} \right|_0 \langle q_i \rangle + \frac{1}{2} \left. \frac{\partial^2 \nu}{\partial q_i^2} \right|_0 \langle q_i^2 \rangle \right] + O(q^3) \tag{1}$$

The first-order term represents the change of atomic equilibrium positions, corresponding to thermal expansion. Here we emphasize that the first-order term is typically smaller than the second-order term, as $\langle q_i \rangle$ originates from the weak phonon anharmonicity. Then, what appears to be a "first-order term" in eq 1 is actually the product of first-order and third-order terms, as a purely harmonic system will have zero thermal expansion with $\langle q_i \rangle = 0$. We evaluate the first-order term through the quasiharmonic approximation[37] as a static lattice expansion effect. The temperature-dependent lattice parameter $a(T)$ of nitrogen-rich diamond is obtained from the previous experiments,[38] and $\nu(a)$ is calculated for different a at the equilibrium atomic configuration. The thermal-expansion contribution to the spectral drift is then:

$$\left. \frac{\partial \nu}{\partial T} \right|_{\text{quasiharmonic}} = \left. \frac{\partial \nu}{\partial a} \right|_{a=a(T)} a(T)\alpha(T) \tag{2}$$

where $\alpha(T)$ is the linear thermal-expansion coefficient at temperature T.

The dominant second-order term represents the atomic vibration around the equilibrium positions caused by phonon excitations at finite temperature. The second-order term is evaluated by the dependence of the spin-transition energy ν on the phonon occupation number n_i = 0, 1, 2... (i is the vibrational mode index), which affects $\langle q_i^2 \rangle$ in eq 1. By evaluating $\langle q_i^2 \rangle$ for a quantum harmonic oscillator (harmonic phonon theory) at thermal equilibrium, $\langle q_i^2 \rangle = \frac{\hbar}{M_i\omega_i}\left(\langle n_i \rangle + \frac{1}{2}\right) = \frac{\hbar}{M_i\omega_i}\left(\frac{1}{e^{\hbar\omega_i/kT} - 1} + \frac{1}{2}\right)$, we obtain

$$\langle \nu \rangle = \nu_0(a(T)) + \sum_i \frac{1}{2} \frac{\partial^2 \nu}{\partial q_i^2} \frac{\hbar}{M_i\omega_i}\left(\frac{1}{e^{\hbar\omega_i/kT} - 1} + \frac{1}{2}\right) \tag{3}$$

where M_i is the mode-specific effective mass (conjugate to the q_i definition) in real-space harmonic lattice dynamics expansion. Here we already included the "first-order" thermal-expansion term in eqs 1 and 2 by taking ν_0 not at the zero-temperature lattice constant a_0 but at finite-temperature lattice parameter $\nu_0 = \nu_0(a(T))$. We notice that the dynamical phonon effect contributes a finite zero-point vibration term to the spin-transition frequency even at zero temperature.

We can gain additional physical intuition of this result by considering the Franck−Condon discussions[39] and graphically analyzing the expected frequency shift, as shown in Figure 1(a). We consider two spin energy levels within vibrational energy levels (n_i = 0, 1, 2,...) associated with orthogonal vibrational wave functions of the ions. Suppose the upper energy surface (red, associated with the higher spin energy) has a slightly softer phonon frequency, which is true on average for the NV^- center. Therefore, the spin-transition energy ν decreases as the phonon number $n_i^{\text{red}} = n_i^{\text{blue}} = n$ increases. Although the typical radio frequency and microwave (MHz to GHz) spin control cannot induce direct transitions between different phonon levels n_i (~THz), these vibration energy levels still affect the average spin-transition frequencies by inducing relatively small shifts in total energy $\left(n_i + \frac{1}{2}\right)\hbar\Delta\omega_i$, where $\Delta\omega_i = \omega_i^{\text{red}} - \omega_i^{\text{blue}}$ is the difference in modal frequency between the upper energy surface (red) and the lower energy surface (blue).

More specifically, the mean value of the spin-transition frequency can be calculated as

$$\begin{aligned} \langle \nu \rangle &= \sum_{\{n_i\}} \frac{e^{-\sum_i \hbar\omega_i(n_i+\frac{1}{2})/kT}}{Z}\left[\nu_0(a(T)) + \sum_i \frac{\Delta\omega_i}{2\pi}\left(n_i + \frac{1}{2}\right)\right] \\ &= \nu_0(a(T)) + \sum_i \frac{\Delta\omega_i}{2\pi}\left(\frac{1}{e^{\hbar\omega_i/kT} - 1} + \frac{1}{2}\right) \end{aligned} \tag{4}$$

As $\Delta\omega_i \ll \omega_i \equiv (\omega_i^{\text{red}} + \omega_i^{\text{blue}})/2$, the expression can be evaluated by the second-order derivative of the spin-transition energy (vertical distance between red and blue) to the normal-mode coordinates $\Delta\omega_i = \frac{\hbar}{2M_i\omega_i}\frac{\partial^2(2\pi\nu)}{\partial q_i^2}$, where $2\pi\hbar\nu = E^{\text{red}} - E^{\text{blue}}$ is the difference in red and blue potential energy surfaces,

https://doi.org/10.1021/acs.jpclett.3c00314
J. Phys. Chem. Lett. 2023, 14, 3266−3273

and we have used the fundamental relation of harmonic oscillators for each phonon mode:

$$M_i\omega_i^2 = \frac{\partial^2 E}{\partial q_i^2} \rightarrow 2M_i\omega_i\Delta\omega_i = \frac{\partial^2(E^{\mathrm{red}} - E^{\mathrm{blue}})}{\partial q_i^2} \tag{5}$$

Thus, this independent derivation from (4) gives

$$\langle\nu\rangle = \nu_0(a(T)) + \sum_i \frac{1}{4\pi M_i\omega_i}\frac{\partial^2(2\pi\hbar\nu)}{\partial q_i^2}\left(\frac{1}{e^{\hbar\omega_i/kT} - 1} + \frac{1}{2}\right) \tag{6}$$

which is identical to eq 3.

The zero-phonon line (ZPL), unlike the spin-transition energies D, A, and Q, will have much larger transition energy/frequency than the vibrational frequency. For ZPL, there is also no vibrational transition (direct mixing with first-order $\hbar\omega_i$), as this is the "zero-phonon" vibronic transition. But the second-order phonon-frequency softening argument due to $n^{\mathrm{blue}} = n \rightarrow n^{\mathrm{red}} = n$ in Figure 1(a) still holds, and therefore, the eq 6 derivation is still valid as well as eq 3. The absolute transition rate can be computed through total vibronic wave function overlap (joint electronic-vibrational wave function overlap between the red and blue)[39].

Thus, the temperature-dependent frequency due to the dynamic-harmonic-phonon effect is given by eq 3, which is the form we will adopt for the numerical computations in this paper. At first, a full phonon calculation is implemented through the phonopy package[40] combined with DFPT implemented in Vienna ab initio simulation package (VASP)[41,42] to derive the frequency ω_i and effective mass M_i of the full phonon spectrum. The second-order derivatives are then calculated by the finite-differential method:

$$\frac{\partial^2\nu}{\partial q_i^2} = \frac{1}{\delta q_i^2}[\nu(\delta q_i) + \nu(-\delta q_i) - 2\nu(0)] + O(\delta q_i^2) \tag{7}$$

where $\nu(q_i)$ is calculated by exerting a small displacement of δq_i relative to the relaxed atomic configuration in the DFT calculations (see Supporting Information (SI) for details[43]).

We simulate the NV^- center in diamond by a 4 × 4 × 4 rhombohedral supercell with the single defect at the center. First, we calculate the zero-temperature electronic structures of the NV^- center for the fully relaxed atomic configuration (Figure 1b). The electronic structure calculation employs the DFT and projector-augmented-wave (PAW) method implemented by VASP. The ground state $^3A_2$ contains electron spin $S = 1$ and ^{14}N nuclear spin $I = 1$, leading to the fine and hyperfine structure shown in Figure 1(c). The spin state splittings originate from three types of interaction: the electron−electron magnetic dipolar interaction $\boldsymbol{D}$, the hyperfine interaction $\boldsymbol{A}$, and the nuclear quadrupole interaction $\boldsymbol{Q}$:[44]

$$\hat{H} = \vec{S}\cdot\boldsymbol{D}\cdot\vec{S} + \vec{S}\cdot\boldsymbol{A}\cdot\vec{I} + \vec{I}\cdot\boldsymbol{Q}\cdot\vec{I} \tag{8}$$

$\boldsymbol{D}$, $\boldsymbol{A}$, and $\boldsymbol{Q}$ are calculated by the first-order perturbation theory to the DFT ground state[33,45−48] (see SI[43] for details). Selecting the C_3 axis of the NV^- center as the z-direction and taking into account that $H_D \gg H_A, H_Q$, the effective Hamiltonian, reduces to[36]

$$\hat{H} = DS_z^2 + QI_z^2 + A_{zz}S_zI_z \tag{9}$$

where $D = \frac{3}{2}D_{zz}$ and $Q = \frac{3}{2}Q_{zz}$ (magnetic field coupling terms are not included). The temperature variations of D, Q, and A_{zz} are then calculated by relating them to transitions ν between two selected spin states (illustrated in Figure 1c). Similarly, the ZPL's temperature dependence is calculated by eq 4 using the ΔSCF method[45,49,50] (see SI[43] for details).

Applying our method to electronic transition, we calculate the temperature dependence of the ZPL and ZFS (Figure 2).

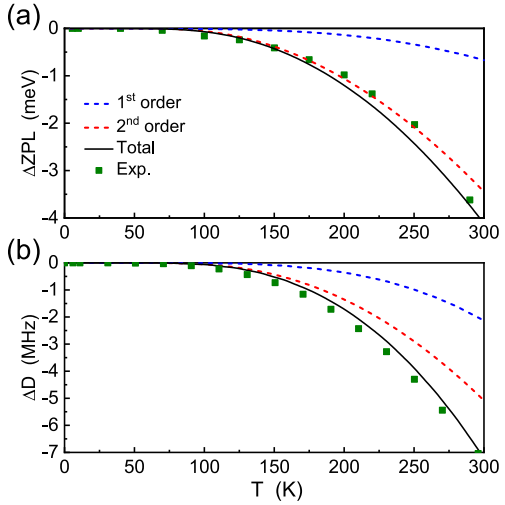

Figure 2. (a) The ZPL and (b) ZFS from simulation and experiment. The blue and red dashed lines represent the first-order (thermal expansion) and second-order (dynamical phonon) effects, respectively. The black line is the total shift from simulation, and the green dots are experimental data points from refs 17 and 31. The well-known first-order effect in (b) is obtained from ref 17.

The "first-order" thermal-expansion effect is, as found in previous computational work,[27,33] far smaller than the experimental results for the measured temperature drifts. This is not surprising, since the quasiharmonic "first-order" is physically a "cubic-order" Grüneisen parameter × "first-order" effect. Including the second-order dynamical phonon effects corrects the discrepancy. The overall simulation results (summation of the first- and second-order) for both quantities are now consistent with prior experimental results. The calculated temperature derivative $\frac{dD}{dT}$ at room temperature is −75.99 kHz/K, consistent with the widely used experimental value of −74.27 kHz/K.[27] Different from ref 17, where the dynamical phonon effect is fitted by experiment, we evaluate the effect in a parameter-free manner from first-principles calculations. Our result indicates that the main mechanism of the temperature dependence of the ZPL and ZFS is the dynamical phonon effect, with a much smaller contribution from the thermal-expansion strain, at least near room temperature. The temperature shift of the ZFS in NV^- centers provides promising prospects for nanothermometry, where the magnitude of $\frac{dD}{dT}$ is crucial for its temperature sensitivity.[6] Our method provides a predictive tool to search for different color centers for optimal temperature sensitivity.

We notice that the method we used to calculate the ZFS (developed in ref 33) does not take an exact estimation to the contribution of the electron wave functions in the atomic core regions. The method also involves errors from the spin contamination issue.[52] Despite this, as the core contribution is estimated to be less than 5%[33] and the predicted response of the ZFS to external perturbations is reasonably consistent with

https://doi.org/10.1021/acs.jpclett.3c00314
J. Phys. Chem. Lett. 2023, 14, 3266−3273

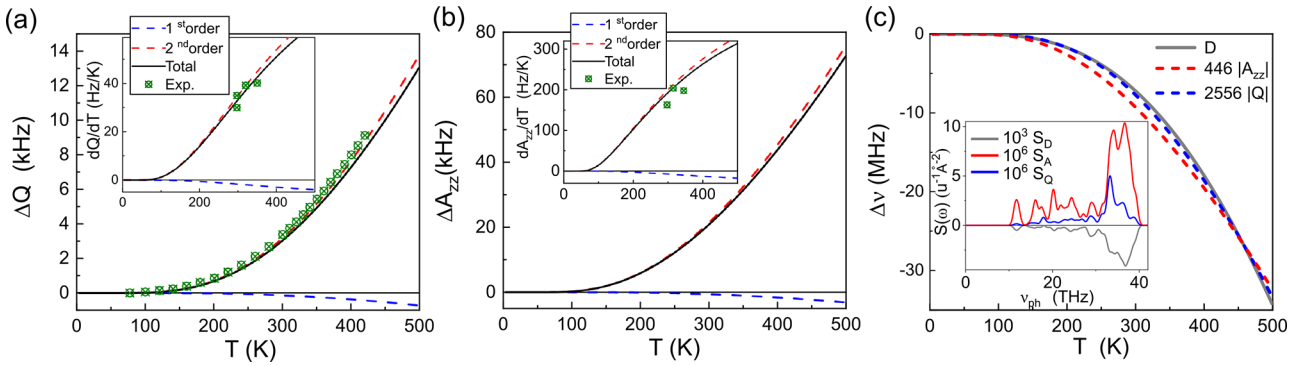

Figure 3. (a) Nuclear quadrupole interaction Q and (b) hyperfine interaction A_{zz} from simulation. The blue, red, and black curves represent the calculated temperature-induced change from the thermal-expansion effect, the second-order vibration effect, and their summation, respectively. The insets are the derivative of Q and A_{zz} results, where the green dots are experimental data obtained from refs 17, 28, 29, and 51. (c) Overlap behavior of $D(T)$, $Q(T)$, and $A_{zz}(T)$ from simulation. The inset shows the spectral density S_D, S_Q, and S_A as defined in eq 10, where Gaussian broadening is applied to the $\delta(\omega - \omega_i)$ for each phonon mode with a width of 2 THz.

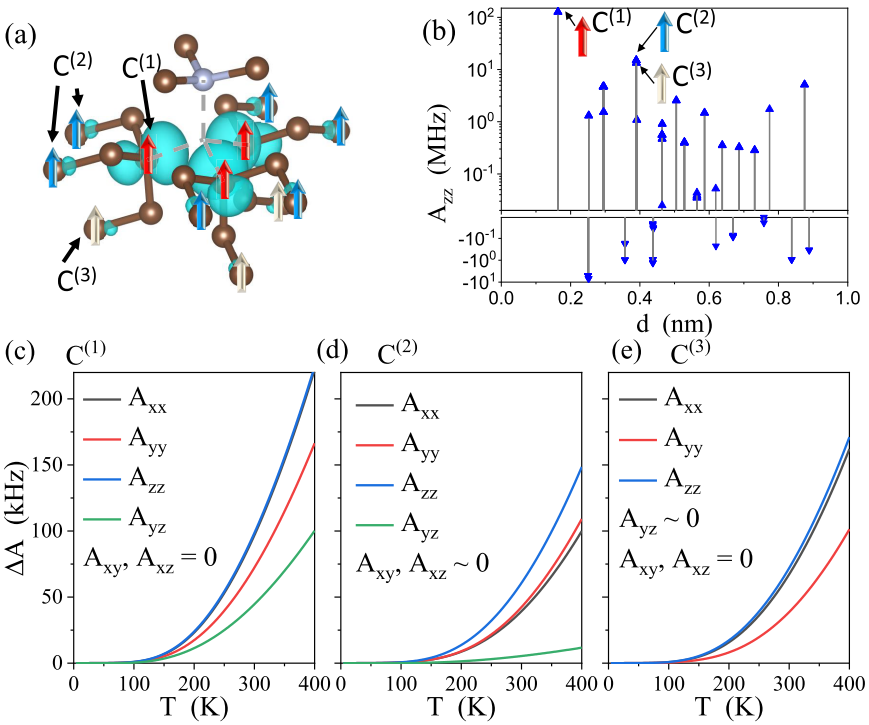

Figure 4. Hyperfine interaction A_{zz} with ^{13}C nuclear spin from simulation. (a) Illustration of the three groups of identical nuclear spins with the strongest hyperfine interaction. (b) A_{zz} for different ^{13}C nuclear spins around the NV^- center plotted against the distance d between the ^{13}C site and the NV^- center. (c) Temperature shifts of different components of the hyperfine tensor $\boldsymbol{A}$ for ^{13}C atoms at different sites. The z-axis orients from the vacancy site to the ^{14}N site, the x-axis is along the vector between the two $C^{(2)}$ atoms pointed by black arrows (toward the upper one), and $\hat{y} = \hat{z} \times \hat{x}$. In the label, $A_{ij} = 0$ means the exact zero by symmetry and $A_{ij} \approx 0$ means numerically almost zero.

experiments in both previous work and our work, we expect the method can approximately output the temperature dependence of the ZFS.

We then calculate the temperature dependence of the nuclear spin interaction. The temperature dependence of ^{14}N-related nuclear spin transition is shown in Figures 3(a,b). Both A_{zz} and Q are negative quantities, and their absolute values decrease with increasing temperature, yielding positive dQ/dT and dA_{zz}/dT. The thermal-expansion contribution to the temperature shifts has an opposite slope with respect to the experiments. The dynamical phonon effect is more than 1 order of magnitude larger than the thermal-expansion effects, so it corrects both the trend and the magnitude, obtaining $\frac{dQ}{dT}$ and $\frac{dA_{zz}}{dT}$ in good agreement with the previous experiments.[17,28,29,51]

A_{zz} is much more sensitive to T than Q. The sensitivity of A_{zz} mainly comes from the Fermi contact term, which is highly sensitive to the atomic displacement in the dynamical phonon effects according to our calculations. In comparison, the electric field gradient (EFG) is relatively insensitive to atomic displacement, so Q has a smaller temperature shift. Therefore, we expect that the higher sensitivity of A_{zz} than Q is also a general behavior in many other color centers. It has been recently proposed that with $\frac{dA_{zz}}{dQ} > 1$, the coherence time of nuclear spin qubits can be robustly protected by at least 1

https://doi.org/10.1021/acs.jpclett.3c00314
J. Phys. Chem. Lett. 2023, 14, 3266−3273

order of magnitude through noise decoupling techniques.[51] The generality of the higher sensitivity of A_{zz} indicates a broad applicability of such a method to various solid state spin defects. The relative shift of the hyperfine transition, $\frac{dA_{zz}}{dT}\frac{1}{A_{zz}}$ approaches 8.9×10^{-5} K^{-1} at room temperature. While the absolute value of the ZFS shift is much larger, the relative frequency change $\frac{dD}{dT}\frac{1}{D} \approx 2.58 \times 10^{-5}$ K^{-1} is smaller than for the hyperfine interaction. Thus, to operate a quantum sensor based on the nuclear spin, it is imperative to recalibrate the temperature effects.[26] The perpendicular hyperfine interaction A_{xx} is also important for nuclear spin dynamics,[36] whose temperature dependence is shown in SI section V.

Previous experimental results had observed a strong, but so-far unexplained, correlation between $D(T)$ and $Q(T)$.[29] Our first-principles results not only confirm such a correlation over a broad temperature range from 100 to 500 K (Figure 3c) but also provide approaches to revealing the underlying mechanism of such a correlation. As the dynamical phonon effects are dominant for all these interactions, we investigate the overlap behavior by defining the spectral density of the second-order derivative of ν as

$$S^i(\omega) = \sum_j \frac{1}{M_j}\frac{\partial^2 \nu^i}{\partial q_j^2}\delta(\omega - \omega_j^i) \tag{10}$$

as shown in the inset of Figure 3(c). The large intensities of S^D, S^Q, and S^A at around 32−38 THz are attributed to the high phonon density of states (DOS)[53] and large second-order derivatives in eq 10 at that frequency range. The ratio between two temperature-induced frequency shifts (second-order) is then a weighted average between their spectral density:

$$\frac{\Delta\nu^1}{\Delta\nu^2} = \frac{\int S^1(\omega) f_{BE}(T, \omega)/\omega d\omega}{\int S^2(\omega) f_{BE}(T, \omega)/\omega d\omega} \tag{11}$$

where f_{BE} is the Bose-Einstein distribution. As the spectral densities S_Q and S_D have a similar shape, the ratio $\Delta Q/\Delta D$ is relatively insensitive to temperature. In comparison, S_A shows a more striking difference, undermining A_{zz}'s overlap with Q and D. Thus, although $A_{zz}(T)$ also shows an approximate correlation with Q and D, it has a relatively larger deviation with a larger slope in the low-temperature region and a smaller slope in the high-temperature region as shown in Figure 3(c). We note that the spectral correlation between different interactions can be quite accurate and paves the way to designing robust coherence protection protocols by refocusing one-interaction variations using other correlated interactions over a broad range of temperatures.[51]

Beyond accurately reproducing experimental results, we can predict the hyperfine temperature shift of ^{13}C nuclear spins around the NV^- center, which have been actively investigated as qubits[30,54−57] (Figure 4a). A_{zz} for ^{13}C atoms at different lattice sites around the NV^- centers is shown in Figure 4b as a function of their distance to the NV^- center, where we identify three groups of equivalent ^{13}C lattice sites with the strongest interaction. The ^{13}C atom at the first-shell lattice sites ($C^{(1)}$) of the NV^- center shows a strong hyperfine splitting of 129 MHz, well consistent with the experimental value of 127 MHz.[30]

The temperature dependence $\Delta \boldsymbol{A}(T)$ of the three groups of ^{13}C lattice sites is shown in Figure 4(c−e). As specifying a given ^{13}C nuclear spin reduces the C_{3v} symmetry, there are more independent components of the hyperfine matrix: $C^{(1)}$ and $C^{(3)}$'s C_{1h} symmetry gives four independent components (with two constraints $A_{xy} = A_{xz} = 0$), and $C^{(2)}$'s C_1 symmetry allows all six components of $\boldsymbol{A}(T)$ to be independent variables. The diagonal components of $\boldsymbol{A}$ are positively related to T for all three groups of lattice sites, exhibiting sensitive temperature dependence with temperature shifts ranging from 39.3 to 98.5 kHz at 300 K. Previously, experimental work on the temperature dependence of the ^{13}C hyperfine interaction did not provide definite results due to the high noise, while a computational study did not consider the second-order dynamical phonon effect.[30] Our results provide a theoretical prediction for $\boldsymbol{A}(T)$ of ^{13}C atoms near NV^- centers, which could be measured by the nuclear spin transition.[51]

In the discussion above, we focus on the temperature shift under thermal equilibrium, but the dynamical phonon effect on spin-transition frequency can be extended to kinetic processes such as nonequilibrium phonon transport. In general, the temperature shift at a single NV^- center measures a linear combination $\hat{O}(r) = \sum_i \frac{\hbar}{2M_i\omega_i}\frac{\partial^2 \nu}{\partial q_i^2}\hat{n}_i(\vec{r})$ of the particle number operators $\hat{n}_i$ of ambient phonons, where the electron or nuclear spin of an NV^- ensemble can probe phonon distribution in the sample. While most materials characterization methods probe the atomic equilibrium position, the second-order temperature shift of spin defects provides a potential route to probe out-of-equilibrium local atomic vibrations.

Our work provides a general scheme to study the temperature dependence of transition frequencies of color centers. An integrated python program that interfaces with VASP and phonopy is made publicly accessible, which can carry out the numerical workflow automatically. Besides the NV^- center, various other color centers such as SiV, SnV, PbV, GeV, and MgV in diamond are also widely studied due to their potential in quantum sensing and communication.[5,58−60] Besides diamond, point defects in silicon,[61−63] silicon carbide,[64−66] Y_2SiO_5,[67] $CaWO_4$ and YVO_4[68,69] also attract broad interests. The temperature dependence data of transition frequency remains lacking for many of these systems. Applying our method to these spin defects can establish a database for temperature-dependent transition frequency of electronic excitation as well as electron and nuclear spin transitions, which provides critical information for searching and designing high-performance quantum devices such as highly sensitive sensors and long-lived memories. Thus this result paves the way to perform a systematic study on the energy levels of point defects targeted for different quantum applications.

Finally, we raise caution that our current codes calculate the ZFS by evaluating the electron spin−spin dipolar interaction term. In some other color center systems (for example, SiV^- center in diamond), the spin−orbit coupling is also an important source of the ZFS.[46] Especially, the spin−orbit coupling is significant in systems with heavy elements like Y_2SiO_5. In order to calculate the temperature-dependent ZFS of these systems, one can incorporate the spin−orbit coupling calculations into our scheme, which is left to future work.

■ ASSOCIATED CONTENT

Data Availability Statement

The codes are available at https://github.com/htang113/First-principles-Calculation-of-the-Temperature-dependent-Transition-Energies-in-Spin-Defects.

https://doi.org/10.1021/acs.jpclett.3c00314
J. Phys. Chem. Lett. 2023, 14, 3266−3273

Supporting Information

The Supporting Information is available free of charge at https://pubs.acs.org/doi/10.1021/acs.jpclett.3c00314.

Additional computational details and supplementary results, including the DFT settings, methods for transition energy calculations, convergence test, and analysis/results of nonsecular terms in the spin Hamiltonian (PDF)

Transparent Peer Review report available (PDF)

AUTHOR INFORMATION

Corresponding Authors

Paola Cappellaro − *Research Laboratory of Electronics, Department of Nuclear Science and Engineering, and Department of Physics, Massachusetts Institute of Technology, Cambridge, Massachusetts 02139, United States;* orcid.org/0000-0003-3207-594X; Email: pcappell@mit.edu

Ju Li − *Department of Nuclear Science and Engineering, Massachusetts Institute of Technology, Cambridge, Massachusetts 02139, United States; Department of Materials Science and Engineering, Massachusetts Institute of Technology, Cambridge, Massachusetts 02139, United States;* orcid.org/0000-0002-7841-8058; Email: liju@mit.edu

Authors

Hao Tang − *Department of Materials Science and Engineering, Massachusetts Institute of Technology, Cambridge, Massachusetts 02139, United States*

Ariel Rebekah Barr − *Department of Materials Science and Engineering, Massachusetts Institute of Technology, Cambridge, Massachusetts 02139, United States*

Guoqing Wang − *Research Laboratory of Electronics and Department of Nuclear Science and Engineering, Massachusetts Institute of Technology, Cambridge, Massachusetts 02139, United States;* orcid.org/0000-0002-1822-8121

Complete contact information is available at: https://pubs.acs.org/10.1021/acs.jpclett.3c00314

Author Contributions

H.T., A.R.B., and G.W. contributed equally.

Notes

The authors declare no competing financial interest.

ACKNOWLEDGMENTS

We thank Haowei Xu, Boning Li, and Yixuan Song for insightful discussions. This work was supported by DTRA (Award No. HDTRA1-20-2-0002) Interaction of Ionizing Radiation with Matter (IIRM) University Research Alliance (URA) and NSF CMMI-1922206. A.R.B. acknowledges support from a National Science Foundation Graduate Research Fellowship under Grant No. DGE-174530. The calculations in this work were performed in part on the Texas Advanced Computing Center (TACC) and MIT engaging cluster.

REFERENCES

(1) Pezzagna, S.; Meijer, J. Quantum computer based on color centers in diamond. *Appl. Phys. Rev.* **2021**, *8*, 011308.

(2) de Leon, N. P.; Itoh, K. M.; Kim, D.; Mehta, K. K.; Northup, T. E.; Paik, H.; Palmer, B.; Samarth, N.; Sangtawesin, S.; Steuerman, D. Materials challenges and opportunities for quantum computing hardware. *Science* **2021**, *372*, eabb2823.

(3) Pfaff, W.; Hensen, B. J.; Bernien, H.; van Dam, S. B.; Blok, M. S.; Taminiau, T. H.; Tiggelman, M. J.; Schouten, R. N.; Markham, M.; Twitchen, D. J.; et al. Unconditional quantum teleportation between distant solid-state quantum bits. *Science* **2014**, *345*, 532−535.

(4) Childress, L.; Taylor, J.; Sørensen, A. S.; Lukin, M. Fault-tolerant quantum communication based on solid-state photon emitters. *Phys. Rev. Lett.* **2006**, *96*, 070504.

(5) Degen, C. L.; Reinhard, F.; Cappellaro, P. Quantum sensing. *Rev. Mod. Phys.* **2017**, *89*, 035002.

(6) Schirhagl, R.; Chang, K.; Loretz, M.; Degen, C. L. Nitrogen-vacancy centers in diamond: nanoscale sensors for physics and biology. *Annu. Rev. Phys. Chem.* **2014**, *65*, 83−105.

(7) Taylor, J. M.; Cappellaro, P.; Childress, L.; Jiang, L.; Budker, D.; Hemmer, P. R.; Yacoby, A.; Walsworth, R.; Lukin, M. D. High-Sensitivity Diamond Magnetometer with Nanoscale Resolution. *Nat. Phys.* **2008**, *4*, 810−816.

(8) Maze, J. R.; Stanwix, P. L.; Hodges, J. S.; Hong, S.; Taylor, J. M.; Cappellaro, P.; Jiang, L.; Dutt, M. V. G.; Togan, E.; Zibrov, A. S.; Yacoby, A.; Walsworth, R. L.; Lukin, M. D. Nanoscale Magnetic Sensing with an Individual Electronic Spin in Diamond. *Nature* **2008**, *455*, 644−647.

(9) Barry, J. F.; Schloss, J. M.; Bauch, E.; Turner, M. J.; Hart, C. A.; Pham, L. M.; Walsworth, R. L. Sensitivity optimization for NV-diamond magnetometry. *Rev. Mod. Phys.* **2020**, *92*, 015004.

(10) Dolde, F.; Fedder, H.; Doherty, M. W.; Nöbauer, T.; Rempp, F.; Balasubramanian, G.; Wolf, T.; Reinhard, F.; Hollenberg, L. C.; Jelezko, F.; et al. Electric-field sensing using single diamond spins. *Nat. Phys.* **2011**, *7*, 459−463.

(11) Wang, N.; Liu, G.-Q.; Leong, W.-H.; Zeng, H.; Feng, X.; Li, S.-H.; Dolde, F.; Fedder, H.; Wrachtrup, J.; Cui, X.-D.; et al. Magnetic criticality enhanced hybrid nanodiamond thermometer under ambient conditions. *Phys. Rev. X* **2018**, *8*, 011042.

(12) Fujiwara, M.; Shikano, Y. Diamond quantum thermometry: From foundations to applications. *Nanotechnology* **2021**, *32*, 482002.

(13) Doherty, M. W.; Struzhkin, V. V.; Simpson, D. A.; McGuinness, L. P.; Meng, Y.; Stacey, A.; Karle, T. J.; Hemley, R. J.; Manson, N. B.; Hollenberg, L. C.; et al. Electronic properties and metrology applications of the diamond NV^- center under pressure. *Phys. Rev. Lett.* **2014**, *112*, 047601.

(14) Ho, K. O.; Leung, M. Y.; Jiang, Y.; Ao, K. P.; Zhang, W.; Yip, K. Y.; Pang, Y. Y.; Wong, K. C.; Goh, S. K.; Yang, S. Probing local pressure environment in anvil cells with nitrogen-vacancy ($N\text{-}V^-$) centers in diamond. *Phys. Rev. Appl.* **2020**, *13*, 024041.

(15) Jarmola, A.; Lourette, S.; Acosta, V. M.; Birdwell, A. G.; Blümler, P.; Budker, D.; Ivanov, T.; Malinovsky, V. S. Demonstration of diamond nuclear spin gyroscope. *Sci. Adv.* **2021**, *7*, eabl3840.

(16) Soshenko, V. V.; Bolshedvorskii, S. V.; Rubinas, O.; Sorokin, V. N.; Smolyaninov, A. N.; Vorobyov, V. V.; Akimov, A. V. Nuclear spin gyroscope based on the nitrogen vacancy center in diamond. *Phys. Rev. Lett.* **2021**, *126*, 197702.

(17) Doherty, M. W.; Acosta, V. M.; Jarmola, A.; Barson, M. S.; Manson, N. B.; Budker, D.; Hollenberg, L. C. Temperature shifts of the resonances of the NV^- center in diamond. *Phys. Rev. B* **2014**, *90*, 041201.

(18) Neumann, P.; Jakobi, I.; Dolde, F.; Burk, C.; Reuter, R.; Waldherr, G.; Honert, J.; Wolf, T.; Brunner, A.; Shim, J. H.; et al. High-precision nanoscale temperature sensing using single defects in diamond. *Nano Lett.* **2013**, *13*, 2738−2742.

(19) Kraus, H.; Soltamov, V.; Fuchs, F.; Simin, D.; Sperlich, A.; Baranov, P.; Astakhov, G.; Dyakonov, V. Magnetic field and temperature sensing with atomic-scale spin defects in silicon carbide. *Sci. Rep.* **2014**, *4*, 05303.

(20) Alkahtani, M.; Cojocaru, I.; Liu, X.; Herzig, T.; Meijer, J.; Küpper, J.; Lühmann, T.; Akimov, A. V.; Hemmer, P. R. Tin-vacancy

in diamonds for luminescent thermometry. *Appl. Phys. Lett.* **2018**, *112*, 241902.
(21) Nguyen, C. T.; Evans, R. E.; Sipahigil, A.; Bhaskar, M. K.; Sukachev, D. D.; Agafonov, V. N.; Davydov, V. A.; Kulikova, L. F.; Jelezko, F.; Lukin, M. D. All-optical nanoscale thermometry with silicon-vacancy centers in diamond. *Appl. Phys. Lett.* **2018**, *112*, 203102.
(22) Toyli, D. M.; de las Casas, C. F.; Christle, D. J.; Dobrovitski, V. V.; Awschalom, D. D. Fluorescence thermometry enhanced by the quantum coherence of single spins in diamond. *Proc. Natl. Acad. Sci. U.S.A.* **2013**, *110*, 8417−8421.
(23) Kucsko, G.; Maurer, P. C.; Yao, N. Y.; Kubo, M.; Noh, H. J.; Lo, P. K.; Park, H.; Lukin, M. D. Nanometre-scale thermometry in a living cell. *Nature* **2013**, *500*, 54−58.
(24) Plakhotnik, T.; Doherty, M. W.; Cole, J. H.; Chapman, R.; Manson, N. B. All-optical thermometry and thermal properties of the optically detected spin resonances of the NV-center in nanodiamond. *Nano Lett.* **2014**, *14*, 4989−4996.
(25) Gottscholl, A.; Diez, M.; Soltamov, V.; Kasper, C.; Sperlich, A.; Kianinia, M.; Bradac, C.; Aharonovich, I.; Dyakonov, V. Sub-nanoscale Temperature, Magnetic Field and Pressure sensing with Spin Centers in 2D hexagonal Boron Nitride. *arXiv*, 2021. arXiv:2102.10890[cond-mat.mtrl-sci].
(26) Fang, K.; Acosta, V. M.; Santori, C.; Huang, Z.; Itoh, K. M.; Watanabe, H.; Shikata, S.; Beausoleil, R. G. High-sensitivity magnetometry based on quantum beats in diamond nitrogen-vacancy centers. *Phys. Rev. Lett.* **2013**, *110*, 130802.
(27) Acosta, V. M.; Bauch, E.; Ledbetter, M. P.; Waxman, A.; Bouchard, L.-S.; Budker, D. Temperature dependence of the nitrogen-vacancy magnetic resonance in diamond. *Phys. Rev. Lett.* **2010**, *104*, 070801.
(28) Soshenko, V. V.; Vorobyov, V. V.; Bolshedvorskii, S. V.; Rubinas, O.; Cojocaru, I.; Kudlatsky, B.; Zeleneev, A. I.; Sorokin, V. N.; Smolyaninov, A. N.; Akimov, A. V. Temperature drift rate for nuclear terms of the NV-center ground-state hamiltonian. *Phys. Rev. B* **2020**, *102*, 125133.
(29) Jarmola, A.; Fescenko, I.; Acosta, V.; Doherty, M.; Fatemi, F.; Ivanov, T.; Budker, D.; Malinovsky, V. Robust optical readout and characterization of nuclear spin transitions in nitrogen-vacancy ensembles in diamond. *Phys. Rev. Res.* **2020**, *2*, 023094.
(30) Barson, M.; Reddy, P.; Yang, S.; Manson, N.; Wrachtrup, J.; Doherty, M. W. Temperature dependence of the ^{13}C hyperfine structure of the negatively charged nitrogen-vacancy center in diamond. *Phys. Rev. B* **2019**, *99*, 094101.
(31) Chen, X.-D.; Dong, C.-H.; Sun, F.-W.; Zou, C.-L.; Cui, J.-M.; Han, Z.-F.; Guo, G.-C. Temperature dependent energy level shifts of nitrogen-vacancy centers in diamond. *Appl. Phys. Lett.* **2011**, *99*, 161903.
(32) Acosta, V. M.; Jarmola, A.; Zipp, L. J.; Ledbetter, M.; Bauch, E.; Budker, D. Broadband magnetometry by infrared-absorption detection of diamond NV centers and associated temperature dependence. *Advances in Photonics of Quantum Computing, Memory, and Communication IV.* **2011**, 79480W.
(33) Ivády, V.; Simon, T.; Maze, J. R.; Abrikosov, I.; Gali, A. Pressure and temperature dependence of the zero-field splitting in the ground state of NV centers in diamond: A first-principles study. *Phys. Rev. B* **2014**, *90*, 235205.
(34) Baroni, S.; Giannozzi, P.; Testa, A. Green's-function approach to linear response in solids. *Phys. Rev. Lett.* **1987**, *58*, 1861.
(35) Nieminen, R. M. Supercell Methods for Defect Calculations. *Theory of Defects in Semiconductors* **2006**, *104*, 29−68.
(36) Doherty, M.; Dolde, F.; Fedder, H.; Jelezko, F.; Wrachtrup, J.; Manson, N.; Hollenberg, L. Theory of the ground-state spin of the NV^- center in diamond. *Phys. Rev. B* **2012**, *85*, 205203.
(37) Togo, A.; Chaput, L.; Tanaka, I.; Hug, G. First-principles phonon calculations of thermal expansion in Ti_3SiC_2, Ti_3AlC_2, and Ti_3GeC_2. *Phys. Rev. B* **2010**, *81*, 174301.
(38) Jacobson, P.; Stoupin, S. Thermal expansion coefficient of diamond in a wide temperature range. *DRM* **2019**, *97*, 107469.
(39) Lax, M. The Franck-Condon principle and its application to crystals. *J. Chem. Phys.* **1952**, *20*, 1752−1760.
(40) Togo, A.; Tanaka, I. First principles phonon calculations in materials science. *Scr. Mater.* **2015**, *108*, 1−5.
(41) Kresse, G.; Furthmüller, J. Efficient iterative schemes for ab initio total-energy calculations using a plane-wave basis set. *Phys. Rev. B* **1996**, *54*, 11169.
(42) Kresse, G.; Joubert, D. From ultrasoft pseudopotentials to the projector augmented-wave method. *Phys. Rev. B* **1999**, *59*, 1758.
(43) See the Supporting Information for details.
(44) Doherty, M. W.; Manson, N. B.; Delaney, P.; Jelezko, F.; Wrachtrup, J.; Hollenberg, L. C. The nitrogen-vacancy colour centre in diamond. *Phys. Rep.* **2013**, *528*, 1−45.
(45) Gali, A.; Fyta, M.; Kaxiras, E. Ab initio supercell calculations on nitrogen-vacancy center in diamond: Electronic structure and hyperfine tensors. *Phys. Rev. B* **2008**, *77*, 155206.
(46) Vahtras, O.; Loboda, O.; Minaev, B.; Ågren, H.; Ruud, K. Ab initio calculations of zero-field splitting parameters. *Chem. Phys.* **2002**, *279*, 133−142.
(47) Petrilli, H. M.; Blöchl, P. E.; Blaha, P.; Schwarz, K. Electric-field-gradient calculations using the projector augmented wave method. *Phys. Rev. B* **1998**, *57*, 14690.
(48) Kuate Defo, R.; Kaxiras, E.; Richardson, S. L. Calculating the hyperfine tensors for group-IV impurity-vacancy centers in diamond using hybrid density functional theory. *Phys. Rev. B* **2021**, *104*, 075158.
(49) Gavnholt, J.; Olsen, T.; Engelund, M.; Schiøtz, J. Δ self-consistent field method to obtain potential energy surfaces of excited molecules on surfaces. *Phys. Rev. B* **2008**, *78*, 075441.
(50) Gali, A.; Janzén, E.; Deák, P.; Kresse, G.; Kaxiras, E. Theory of spin-conserving excitation of the N-V^- center in diamond. *Phys. Rev. Lett.* **2009**, *103*, 186404.
(51) Wang, G.; Barr, A.; Tang, H.; Chen, M.; Li, C.; Xu, H.; Li, J.; Cappellaro, P. Characterizing temperature and strain variations with qubit ensembles for their robust coherence protection. *arXiv*, 2022; arXiv:2205.02790[quant-ph].
(52) Montoya, A.; Truong, T. N.; Sarofim, A. F. Spin contamination in hartree- fock and density functional theory wavefunctions in modeling of adsorption on graphite. *J. Phys. Chem. A* **2000**, *104*, 6108−6110.
(53) Zhang, J.; Wang, C.-Z.; Zhu, Z.; Dobrovitski, V. Vibrational modes and lattice distortion of a nitrogen-vacancy center in diamond from first-principles calculations. *Phys. Rev. B* **2011**, *84*, 035211.
(54) Maurer, P. C.; Kucsko, G.; Latta, C.; Jiang, L.; Yao, N. Y.; Bennett, S. D.; Pastawski, F.; Hunger, D.; Chisholm, N.; Markham, M.; et al. Room-temperature quantum bit memory exceeding one second. *Science* **2012**, *336*, 1283−1286.
(55) Dréau, A.; Spinicelli, P.; Maze, J.; Roch, J.-F.; Jacques, V. Single-shot readout of multiple nuclear spin qubits in diamond under ambient conditions. *Phys. Rev. Lett.* **2013**, *110*, 060502.
(56) Shim, J.; Niemeyer, I.; Zhang, J.; Suter, D. Room-temperature high-speed nuclear-spin quantum memory in diamond. *Phys. Rev. A* **2013**, *87*, 012301.
(57) Abobeih, M.; Randall, J.; Bradley, C.; Bartling, H.; Bakker, M.; Degen, M.; Markham, M.; Twitchen, D.; Taminiau, T. Atomic-scale imaging of a 27-nuclear-spin cluster using a quantum sensor. *Nature* **2019**, *576*, 411−415.
(58) Thiering, G.; Gali, A. Ab initio magneto-optical spectrum of group-IV vacancy color centers in diamond. *Phys. Rev. X* **2018**, *8*, 021063.
(59) Lühmann, T.; John, R.; Wunderlich, R.; Meijer, J.; Pezzagna, S. Coulomb-driven single defect engineering for scalable qubits and spin sensors in diamond. *Nat. Commun.* **2019**, *10*, 4956.
(60) Pershin, A.; Barcza, G.; Legeza, Ö.; Gali, A. Highly tunable magneto-optical response from magnesium-vacancy color centers in diamond. *npj Quantum Inf.* **2021**, *7*, 99.
(61) Zwanenburg, F. A.; Dzurak, A. S.; Morello, A.; Simmons, M. Y.; Hollenberg, L. C.; Klimeck, G.; Rogge, S.; Coppersmith, S. N.;

https://doi.org/10.1021/acs.jpclett.3c00314
J. Phys. Chem. Lett. 2023, 14, 3266−3273

Eriksson, M. A. Silicon quantum electronics. *Rev. Mod. Phys.* **2013**, *85*, 961.
(62) Hensen, B.; Wei Huang, W.; Yang, C.-H.; Wai Chan, K.; Yoneda, J.; Tanttu, T.; Hudson, F. E.; Laucht, A.; Itoh, K. M.; Ladd, T. D.; et al. A silicon quantum-dot-coupled nuclear spin qubit. *Nat. Nanotechnol.* **2020**, *15*, 13−17.
(63) Petit, L.; Boter, J.; Eenink, H.; Droulers, G.; Tagliaferri, M.; Li, R.; Franke, D.; Singh, K.; Clarke, J.; Schouten, R.; et al. Spin lifetime and charge noise in hot silicon quantum dot qubits. *Phys. Rev. Lett.* **2018**, *121*, 076801.
(64) Castelletto, S.; Boretti, A. Silicon carbide color centers for quantum applications. *J. Phys. photonics* **2020**, *2*, 022001.
(65) Babin, C.; Stöhr, R.; Morioka, N.; Linkewitz, T.; Steidl, T.; Wörnle, R.; Liu, D.; Hesselmeier, E.; Vorobyov, V.; Denisenko, A.; et al. Fabrication and nanophotonic waveguide integration of silicon carbide colour centres with preserved spin-optical coherence. *Nat. Mater.* **2022**, *21*, 67−73.
(66) Anderson, C. P.; Glen, E. O.; Zeledon, C.; Bourassa, A.; Jin, Y.; Zhu, Y.; Vorwerk, C.; Crook, A. L.; Abe, H.; Ul-Hassan, J.; et al. Five-second coherence of a single spin with single-shot readout in silicon carbide. *Sci. Adv.* **2022**, *8*, eabm5912.
(67) Zhong, T.; Rochman, J.; Kindem, J. M.; Miyazono, E.; Faraon, A. High quality factor nanophotonic resonators in bulk rare-earth doped crystals. *Opt. Express* **2016**, *24*, 536−544.
(68) Le Gall, C. Clock qubit conducts nuclear ensemble. *Nat. Phys.* **2022**, *18*, 230.
(69) Ruskuc, A.; Wu, C.-J.; Rochman, J.; Choi, J.; Faraon, A. Nuclear spin-wave quantum register for a solid-state qubit. *Nature* **2022**, *602*, 408−413.

NOTE ADDED AFTER ASAP PUBLICATION

Additional text corrections were made on March 30, 2023.

https://doi.org/10.1021/acs.jpclett.3c00314
J. Phys. Chem. Lett. 2023, 14, 3266−3273

Supporting Information: First-principles Calculation of the Temperature-dependent Transition Energies in Spin Defects

Hao Tang,[1,*] Ariel Rebekah Barr,[1,*] Guoqing Wang,[2,3,*] Paola Capellero,[2,3,4,†] and Ju Li[1,3,‡]

[1] *Department of Materials Science and Engineering, Massachusetts Institute of Technology, MA 02139, USA*
[2] *Research Laboratory of Electronics, Massachusetts Institute of Technology, Cambridge, MA 02139, USA*
[3] *Department of Nuclear Science and Engineering, Massachusetts Institute of Technology, Cambridge, MA 02139, USA*
[4] *Department of Physics, Massachusetts Institute of Technology, Cambridge, MA 02139, USA*

(Dated: March 8, 2023)

I. DETAILS OF FIRST-PRINCIPLES CALCULATION

The electronic structure calculation employs the projector-augmented-wave (PAW) method implemented by the Vienna ab-initio simulation package (VASP) with a cut-off energy of 520 eV [1, 2]. Spin-unrestricted calculations are implement using the generalized gradient approximation (GGA) with the Perdew-Burke-Ernzerhof (PBE) functional for electron exchange-correlation [3] in the calculation of atomic relaxation, density functional perturbation theory (DFPT), D, Q, and A matrix. The k-point mesh is sampled by the Monkhorst-Pack method [4] with a seperation of 0.2 rad/Å^{-1} ($3\times3\times3$ k-point mesh in the supercell). The energy of electronic iterations converge to 10^{-7} eV and force on atoms converge to 0.01 eV/Å.

The phonon calculation is implemented in the $4\times4\times4$ rhombohedral supercell with only Γ k-point. 381 phonon modes are obtained at Γ k-point, including 3 trivial modes corresponding to overall translation. The trivial modes have no contribution to Eq. (3) in the main text, as the overall translation of the system does not change any transition energy. All the 378 non-trivial phonon modes are then used to calculate the second-order derivative according to Eq. (3) in the main text. In Eq. (3), the step of displacement δq_i is set as 0.1 Å in the NV center calculation. We tested that using $\delta q_i = 0.05$ Å gives almost the same temperature dependence, confirming the convergence of our results to δq_i. We mention that numerically, $\delta q_i = 0.1$ Å is not a large value as it appears to be, as this magnitude of displacement is distributed to all the 127 atoms in the supercell, and the displacement of each atom is in a proper range.

II. CALCULATION OF D, Q, AND A

The first term in Eq. (8) in the main text originates from the electron spin-spin magnetic dipolar interaction from the Kohn-Sham orbitals [5]:

$$D_{ij} = \frac{\mu_0 g_e^2 \mu_B^2}{4\pi} \sum_{a<b} \chi_{ab} \left\langle \Psi_{ab} \left| \frac{r^2\delta_{ij} - 3r_i r_j}{r^5} \right| \Psi_{ab} \right\rangle \quad (1)$$

where μ_0, μ_B, g_e are the magnetic constant, Bohr magneton, and Landé factor of electron, respectively. The summation goes through all electron pairs (a, b). Ψ_{ab} are particle determinant wave functions from the Kohn-Sham ground state and χ_{ab} equals +1/-1 when the states a and b have the same/different spin.

The hyperfine constant (the 2$^{\text{nd}}$ term in Eq. (8) in the main text) is a summation of the Fermi contact contribution and dipolar contribution:

$$A_{ij} = \frac{\mu_0 g_e g_I \mu_B \mu_I}{\langle S_z \rangle} \times [\frac{2}{3}\delta_{ij}\rho_s(\mathbf{R}_I) + \frac{1}{4\pi}\int \frac{\rho_s(\mathbf{r}+\mathbf{R}_I)}{r^3}\frac{3r_i r_j - \delta_{ij}r^2}{r^2} d\mathbf{r}] \quad (2)$$

where g_I, μ_I, and R_I are the g-factor, nuclear magneton, and coordinate of nuclear spin, ρ_s is the electron spin density from the DFT ground state. In the NV center calculation, we use the g-factor of $g_I = 3.077 \times \frac{h}{\mu_B}$ MHz/T for ^{14}N and $g_I = 10.7084 \times \frac{h}{\mu_B}$ MHz/T for ^{13}C.

The nuclear quadrupole interaction is calculated through the electric field gradient (EFG) $V_{ij} = \partial_i E_j$ from the electron density $\rho(r)$:

$$V_{ij} = \frac{e}{4\pi\epsilon_0}[-\int \rho(r+R_I)\frac{3r_i r_j - \delta_{ij}r^2}{r^5}dr + \sum_{I'} Z_{I'}\frac{3R_{II',i}R_{II',j} - \delta_{ij}R_{II'}^2}{R_{II'}^5}] \quad (3)$$

where e, ϵ_0, Z'_I, R_I, and $R_{II'}$ are the electron charge, vacuum dielectric constant, nuclear charge, position of nucleus, and relative coordinate between nucleus I' and I. The Q matrix is then calculated by the three principal axis system (PAS) eigenvalues $V_{1,2,3}$ of the EFG:

$$Q_{ij} = \frac{eQ_I}{4I(2I-1)}\begin{bmatrix} V_1 - V_2 - V_3 & 0 & 0 \\ 0 & -V_1 + V_2 - V_3 & 0 \\ 0 & 0 & 2V_3 \end{bmatrix} \quad (4)$$

* These authors contributed equally.
† pcappell@mit.edu
‡ liju@mit.edu

where Q_I is the nuclear quadrupole moment. In the NV center calculation, we use the ^{14}N nuclear quadrupole moment $Q_I = 20.44\ e{\cdot}\mathrm{mb}$.

In the principal axis coordinates, Eq. (8) in the main text is converted to:

$$\hat{H}_D = D[S_z^2 - \frac{1}{3}S(S+1) + \frac{\epsilon}{3}(S_+^2 + S_-^2)] \quad (5)$$

$$\hat{H}_Q = Q[I_z^2 - \frac{1}{3}I(I+1) + \frac{\eta}{3}(I_+^2 + I_-^2)] \quad (6)$$

$$\hat{H}_A = A_{zz}S_zI_z + A_{xx}S_xI_x + A_{yy}S_yI_y \quad (7)$$

where $D = \frac{3}{2}D_{zz}$ and $Q = \frac{3}{2}Q_{zz}$ are the splitting energy, and $\epsilon = (D_{xx} - D_{yy})/D_{zz}$ and $\eta = (Q_{xx} - Q_{yy})/Q_{zz}$ are the asymmetric coefficients. Applying to an uniaxial system like NV-center under zero strain, we select the C_3 axis as z-direction and the effective Hamiltonian reduces to (considering $H_D \gg H_A, H_Q$) Eq. (9) in the main text.

III. CALCULATION OF THE TEMPERATURE-DEPENDENT ZPL

Although the ZPL is not spin-transition, its temperature dependence can be calculated by the same theoretical framework. The only difference is that the energy levels of the excited state and ground state have a large separation of 1.945 eV, so their difference can no longer be evaluated perturbatively. Compared with the spin transition where the transition energy is far smaller than the phonon energy, here the electronic transition energy is far larger than the phonon energy.

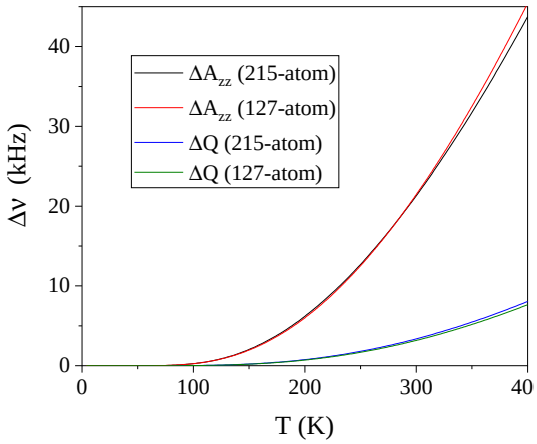

FIG. 1. Convergence test of the temperature dependence of A_{zz} and Q of the ^{14}N nuclear spin in NV centers. The black/blue and red/green curves represent the temperature drifts of A_{zz}/Q of the ^{14}N atom calculated by the 215-atom rhombohedral supercell and 127-atom cubic supercell, respectively

The calculation is implemented through evaluating Eq. (4) in the main text. At first, we use the Δ SCF method [6] to calculate the relaxed atomic structure and electronic structures of the excited states, where one electron is placed in a high-lying Kohn-Sham orbital. In the NV center calculation, this is realized by fixing the electron occupancy according to the ^3E excited state's a_1e^3 molecular orbital configuration as in ref. [7]. For the two degenerate excited orbitals (e_x, e_y), we use (1, 0) occupancy for the excited state as the previous works [7, 8]. The same electron occupancy is set for all k points in the supercell calculation, yielding the ^3E state with one excited electron in each NV center, or namely, one excited electron in each supercell. The phonon spectral of the excited states is then calculated, deriving a series of excited state phonon frequency ω_i^e. Combining with the ground state phonon frequency ω_i^g, we derive $\Delta\omega_i$ in Eq. (4) in the main text. ω_i in the equation is set as the ground state phonon frequency, as phonon exhibits the Boson distribution according to the ground state phonon spectral in the ZPL measurement. The first-order contribution from $\nu_0(T)$ is directly calculated through the excitation energy calculation under lattice expansion by the Δ SCF method.

We notice that calculating the temperature dependence of the ZPL is less computationally expansive than calculating that of the spin interaction terms. That is because the atomic vibration frequency difference of the two electronic states in the ZPL can be directly evaluated by phonon calculations. In comparison, a scheme to evaluate the atomic vibration frequency difference between two spin states is lacking to our knowledge. Developing such schemes can potentially benefit the spin-phonon interaction calculations, which is left to future work.

IV. CONVERGENCE TEST OF THE SUPERCELL SIZE

Here we conducted convergence test to show that the 127-atom $4 \times 4 \times 4$ rhombohedral supercell we used for NV centers can derive temperature dependence reasonably convergent against supercell size. The temperature dependence of A_{zz} and Q is calculated by both the 127-atom supercell and a 216-atom cubic supercell, as shown in Fig. 1. The temperature dependence calculated by different supercell is well consistent, supporting that the 127-atom supercell can derive temperature dependence with reasonable convergence. As the computational cost of the temperature dependence calculation grows dramatically with the supercell size, we recommend the 127-atom supercell based on our test results to people who intend to use our method.

V. TEMPERATURE DEPENDENCE OF COMPLETE SPIN INTERACTION MATRIX

In addition to the secular terms in Eq. (9) in the main text, there are also other components of the matrix D, A,

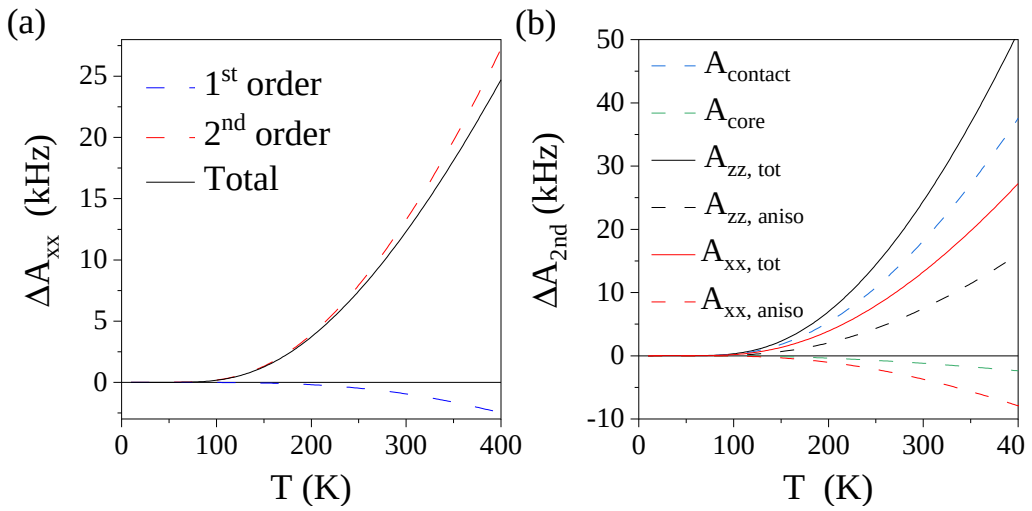

FIG. 2. (a) Temperature dependence of A_{xx} of the ^{14}N nuclear spin in NV centers. The blue dashed line, red dashed line, and black line represent the 1^{st} order, 2^{nd} order, and total temperture drift. (b) Fermi contact (denoted as contact), core correction (denoted as core), and dipolar interaction (denoted as aniso) terms of the 2^{nd}-order hyperfine interaction.

and Q in Eq. (8) in the main text, which are also important to characterize the spin dynamics of the system [9]. We include a complete temperature dependence analysis of these matrix.

We first notice that the temperature effects do not break the C_{3v} symmetry of the system. Therefore, the matrix D and A, Q for the ^{14}N nuclear spin still keep the symmetric form:

$$\begin{aligned}\hat{H}_D(T) &= D(T)\begin{bmatrix}-\frac{1}{3} & 0 & 0\\ 0 & -\frac{1}{3} & 0\\ 0 & 0 & \frac{2}{3}\end{bmatrix},\\ \hat{H}_Q(T) &= Q(T)\begin{bmatrix}-\frac{1}{3} & 0 & 0\\ 0 & -\frac{1}{3} & 0\\ 0 & 0 & \frac{2}{3}\end{bmatrix},\\ \hat{H}_A(T) &= \begin{bmatrix}A_{xx}(T) & & \\ 0 & A_{xx}(T) & 0\\ 0 & 0 & A_{zz}(T)\end{bmatrix}\end{aligned} \tag{8}$$

Notice that the asymmetry factors η and ϵ in Eq. (5,6) are zero at both zero temperature and finite temperature. The only non-secular term that is not reported in the main text is $A_{xx}(T)$, the perpendicular hyperfine interaction (denoted as $A_\perp$ in some literature [9]).

The temperature dependence $A_{xx}(T)$ is plotted in Fig. 2a. We plot the symmetrized temperature drift $\frac{1}{2}(A_{xx} + A_{yy})$, as the calculated $A_{xx}(T)$ and $A_{yy}(T)$ have slight difference due to numerical error. As $A_{zz}(T)$, the $A_{xx}(T)$ have a dominant positive contribution from the 2^{nd} order effect and a smaller negative contribution from the 1^{st} order effect. The total temperature drift $\Delta A_{xx}(T)$ is smaller than $\Delta A_{zz}(T)$ in the studied temperature range. As the temperature effect on $A_{xx}(T)$ has not been reported by experiments, this data also provides a prediction.

In Fig. 2b, we plot different contributing terms of the temperature drift ΔA_{xx} and ΔA_{zz}: the fermi contact term (the first term in Eq. (2)) and its core correction, and the dipolar interaction term (the second term in Eq. (2)).

[1] G. Kresse and J. Furthmüller, Efficient iterative schemes for ab initio total-energy calculations using a plane-wave basis set, Phys. Rev. B **54**, 11169 (1996).

[2] G. Kresse and D. Joubert, From ultrasoft pseudopotentials to the projector augmented-wave method, Phys. Rev. B **59**, 1758 (1999).

[3] J. P. Perdew, K. Burke, and M. Ernzerhof, Generalized gradient approximation made simple, Phys. Rev. Lett. **77**, 3865 (1996).

[4] H. J. Monkhorst and J. D. Pack, Special points for brillouin-zone integrations, Phys. Rev. B **13**, 5188 (1976).

[5] V. Ivády, T. Simon, J. R. Maze, I. Abrikosov, and A. Gali, Pressure and temperature dependence of the zero-field splitting in the ground state of nv centers in diamond: A first-principles study, Phys. Rev. B **90**, 235205 (2014).

[6] J. Gavnholt, T. Olsen, M. Engelund, and J. Schiøtz, Δ self-consistent field method to obtain potential energy surfaces of excited molecules on surfaces, Phys. Rev. B **78**, 075441 (2008).

[7] A. Gali, E. Janzén, P. Deák, G. Kresse, and E. Kaxiras, Theory of spin-conserving excitation of the n-v^- center in diamond, Phys. Rev. Lett. **103**, 186404 (2009).

[8] T. A. Abtew, Y. Sun, B.-C. Shih, P. Dev, S. Zhang, and P. Zhang, Dynamic jahn-teller effect in the nv^- center in diamond, Phys. Rev. Lett. **107**, 146403 (2011).

[9] M. Doherty, F. Dolde, H. Fedder, F. Jelezko, J. Wrachtrup, N. Manson, and L. Hollenberg, Theory of the ground-state spin of the nv^- center in diamond, Phys. Rev. B **85**, 205203 (2012).